COMPUTATIONAL MECHANICS
WCCM VI in conjunction with APCOM'04, *Sept. 5-10, 2004, Beijing, China*

Numerical Simulation of Heat Transfer and Kinetics in the Bulk Growth of Silicon Carbide

Zibing Zhang, Jing Lu, Qisheng Chen *

Institute of Mechanics, Chinese Academy of Sciences, 15 Bei Si Huan Xi Road, Beijing 100080, China
e-mail: qschen@imech.ac.cn

Abstract The growth process of 2-inch silicon carbide (SiC) single crystals by the physical vapor transport method (or modified Lely method) has been modeled and simulated. The comprehensive process model incorporates the calculations of radio frequency (RF) induction heating, heat and mass transfer and growth kinetics. The transport equations for electromagnetic field, heat transfer, and species transport are solved using a finite volume-based numerical scheme called MASTRAPP (Multizone Adaptive Scheme for Transport and Phase Change Process). Temperature distribution for a 2-inch growth system is calculated, and the effects of induction heating frequency and current on the temperature distribution and growth rate are investigated. The predicted results have been compared with the experimental data.

Key words: silicon carbide, physical vapor transport, process modeling, finite volume method

INTRODUCTION

Silicon carbide (SiC) is a promising semiconductor material for electronic and optoelectronic devices which can operate in high power, high temperature, high frequency and intense radiation conditions. The bulk growth of SiC by physical vapor transport (PVT), or modified Lely method involves many important physical phenomena, such as electromagnetic field, radio frequency induction heating, conduction and radiation heat transfer, sublimation and condensation, mass transport, and so on. Since in-situ measurement of temperature, flow velocity, species concentration, and growth rate is extremely difficult, physics-based process modeling is a powerful tool by which one can develop a better understanding of the transport phenomena in a SiC growth system. It can help us to design efficient growth furnaces and to reduce micropipes and defect densities in as-grown crystals [1] .

In recent years, different growth models have been proposed by several groups [2-8]. Hofmann et al. [2] modeled the temperature distributions in a growth system with growth temperature of 2573 K and system pressure of up to 3500 Pa. Pons et al. [3] calculated the electromagnetic field and temperature distribution. The calculated temperatures at the seed and powder surfaces are 2920 K and 3020 K, respectively, while the temperatures measured at the top and bottom of the crucible are 2390 K and 2500 K, respectively, and the maximum temperature of the insulation foam on its periphery is about 1000 K. Müller et al. [4] calculated the temperature distributions in an inductively heated SiC growth reactor with growth temperatures in the range of 2373-2673 K, and found that the temperatures in the powder are highly nonuniform with radial variations of 30-50 K along the powder surface. Karpov et al. [5] predicted the growth rate in the growth of SiC in tantalum container. Chen et al. [6] proposed a kinetics model for SiC vapor growth, predicted growth rate as a function of temperature, temperature gradient and inert gas pressure. Selder et al. [7] introduced a modeling approach for the simulation of heat and mass transfer during SiC bulk crystal growth and compared the calculated results with the experimental data. Råback et al. [8] presented a model for the growth rate of SiC sublimation process and estimated the parametric dependencies of the growth rate. Ma et al. [9] modeled the thermal stresses in the growing crystal in a

growth system, and the growth pressure is 1333 Pa and the temperature at the bottom of crucible is 2200° C.

The growth process in a 2-inch growth system is modeled in this paper. A coupled, high-resolution transport model is developed to predict the electromagnetic field, heat and mass transfer in the growth system and the growth rate. Temperature distributions for different currents and frequencies are calculated, and the effects of induction heating frequency and current on the temperature distribution and growth rate are investigated.

MATHEMATICAL MODEL AND NUMERICAL METHOD

A typical SiC growth system is shown in Fig. 1. It consists of an RF copper coil, quartz tube, graphite susceptor, graphite insulation, crucible, and some other components. The crucible is filled with SiC powder charge, and a SiC seed is placed on the bottom of the lid of the crucible. The SiC charge is heated by induction heating. When reaching the growth temperature, it began to sublimate and deposit on the seed surface.

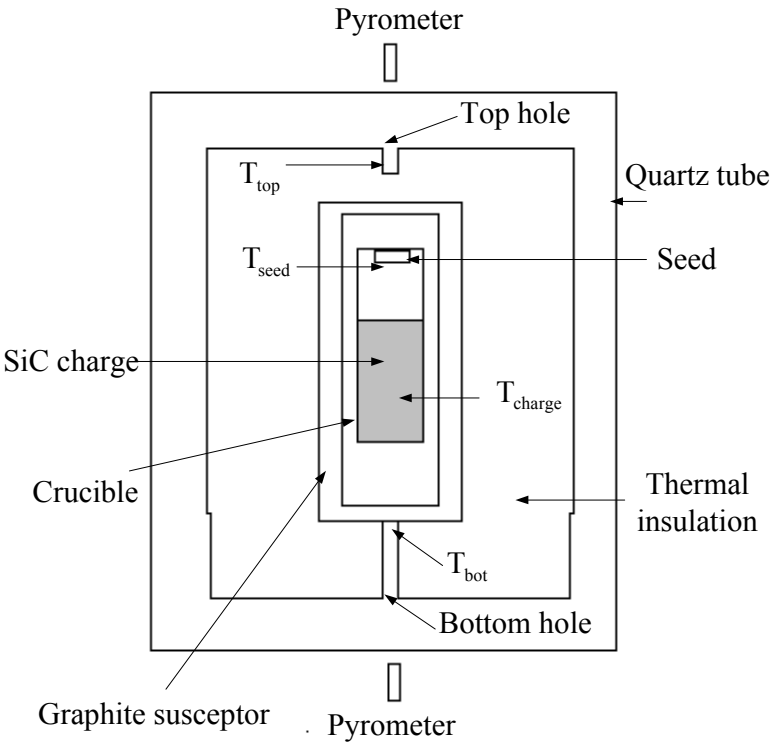

Fig.1 Schematic of the Growth System

1. Electromagnetic Field The electromagnetic field produced by RF induction heating (Fig. 1) can be calculated by solving the Maxwell's equations. For low frequency ($f < 1MHz$), the Maxwell's equations can be simplified using a quasi-steady state approximation which assumes that the current in the coil is time-harmonic, and heat in the graphite susceptor is only generated by eddy currents [9]. Consequently the magnetic flux density, B, can be expressed as the curl of a magnetic vector potential, $\mathbf{B} = \nabla \times \mathbf{A}$. The Maxwell equations can then be written in terms of the vector potential, **A** [7]

$$\nabla \times \left(\frac{1}{\mu_{\mathrm{m}}} \nabla \times \mathbf{A} \right) + \varepsilon_{\mathrm{m}} \frac{\partial^2 \mathbf{A}}{\partial t^2} + \sigma_{\mathrm{c}} \frac{\partial \mathbf{A}}{\partial t} = \mathbf{J}_{\mathrm{coil}} \tag{1}$$

where μ_m is the magnetic permeability, ε_m is the permittivity, σ_c is the electrical conductivity, and $\mathbf{J}_{\mathrm{coil}}$ is the current density in the coil. It is assumed that the coil and the magnetic field are axisymmetric, so that both **A** and the current density $\mathbf{J}_{\mathrm{coil}}$ have only one angular component with an exponential form,

$$\mathbf{A} = \begin{Bmatrix} 0 \\ A_0 e^{i\omega t} + cc \\ 0 \end{Bmatrix} \text{ and } \mathbf{J}_{coil} = \begin{Bmatrix} 0 \\ J_0 e^{i\omega t} + cc \\ 0 \end{Bmatrix} \tag{2}$$

Where i is the complex unit, ω is the angular frequency and cc denotes the complex conjugate. The final equation for vector potential, A_0, is obtained by substituting Eq. (2) into Eq. (1),

$$\left(\frac{\partial^2}{\partial r^2} + \frac{1}{r}\frac{\partial}{\partial r} - \frac{1}{r^2} + \frac{\partial^2}{\partial z^2} \right) \left(\frac{A_0}{\mu_m} \right) + \varepsilon_m \omega^2 A_0 - i\omega\sigma_c A_0 = -J_0 \tag{3}$$

In an axisymmetric system, the following boundary conditions can be imposed on equation (3),

$$A_0=0, \quad \text{at } r=0 \text{ and } r^2 + z^2 \to \infty \tag{4}$$

After solving Eq. (3) for the vector potential, A_0, the generated heat power in the graphite susceptor can be obtained using the eddy current theory,

$$q'''_{eddy} = \frac{1}{2}\sigma_c \omega^2 A_0 A_0^* \tag{5}$$

where * denotes the complex conjugate.

2. Energy Transport Equation According to the scale analysis, [10], the heat transfer by convective flow can be negligible for a 2-inch growth system for the first order approximation. Temperature distribution in the growth system is calculated by solving the energy transport equation, which is obtained by using a conduction-radiation model, and can be expressed as,

$$(\rho c_{\mathrm{p}})_{\mathrm{eff}} \frac{\partial T}{\partial t} = \nabla \cdot (k_{\mathrm{eff}} \nabla T) + q'''_{\mathrm{eddy}} - (q''_{\mathrm{radi}} + q''_{\mathrm{insu}}) \delta A / \delta V \tag{6}$$

where $(\rho c_{\mathrm{p}})_{\mathrm{eff}}$ and k_{eff} are local effective heat capacity and conductivity, respectively, δA and δV are the area of a finite volume face within the radiation surface and the finite volume adjacent to the radiation surface, respectively. In Eq. (6) q'''_{radi} is the radiative heat flux normal to the radiation surface, and q''_{insu} is the radiative heat flux on the outer surfaces of insulation. The detail expressions of these terms have been given in [11].

It is assumed that the temperature distribution is axisymmetric, hence at the central axis,

$$\frac{\partial T}{\partial r} = 0 \quad \text{at} \quad r=0 \tag{7}$$

And the ambient temperature is set as,

$$T_\infty = 293K \tag{8}$$

3. Growth Kinetics During the sublimation process, the SiC charge decomposes into various species, and the main components of the evaporation of SiC are Si, SiC_2, Si_2C and SiC. The content of the other components of evaporation (Si_2, C, C_2, C_3) in the vapor is insignificant and can be neglected. It is assumed that the local thermodynamic equilibrium is established during the sublimation process, and then the partial pressures of different vapor species can be obtained [11]. Based on the scale analysis performed by Chen et al. [10], mass transport by natural convection is insignificant. Thus the transport of species from the charge to the seed is determined mainly by the diffusion and Stefan flow. Stefan flow is caused by the volume change during the evaporation of the SiC powder. The vapor species becomes supersaturated near the seed where the temperature is lower than that in the charge.

Because of the lack of carbon species near the seed and since SiC vapor pressure is very small, only the following reaction is considered important for the deposition process [11],

$$2SiC(s) \Leftrightarrow SiC_2(g) + Si(g) \tag{9}$$

where subscripts s, g denote solid and gas, respectively.
The equilibrium constant for the above reaction can be calculated from the equation of equilibrium,

$$K = \exp(-\Delta G_T^0 / RT) \tag{10}$$

where R is the universal gas constant, and ΔG_T^0, the change in isobaric-isothermal Gibbs function [10].
Thermodynamic analysis shows that the vapor becomes silicon rich at temperatures below 2546 K, and SiC_2 rich at temperatures above 2900 K. The rate-determining species, A, is therefore chosen as SiC_2 at T<2546 K, as Si at T>2900 K, and either of the two for 2546 K<T<2900 K. Introducing z'coordinate, which is set as 0 at the charge surface, and L at the seed, the vapor pressures of various species can be calculated as functions of z'. To develop a growth kinetics model, we assume that the species transport rate near the seed is proportional to the supersaturation of the rate-determining species A,

$$J_A = \chi_A (p_A(L) - p_A^*(L)) \tag{11}$$

where p_A^* is the equilibrium vapor pressure of gaseous A, the value of which is given in [1], and $\chi_A = 1/\sqrt{2\pi M_A RT}$. The SiC_2 and Si vapors are assumed to have an identical transport rate, i.e., $J_{SiC_2} = J_{Si}$, which yields the growth rate of SiC crystal as,

$$G_{SiC} = \frac{2M_{SiC}}{\rho_{SiC}} \chi_A \left[p_A(L) - p_A^*(L) \right] \tag{12}$$

For detailed formulations, one can refer to [10].

4. Numerical Method The transport equations for electromagnetic field, heat transfer, and species transport are solved using a finite volume-based numerical scheme called MASTRAPP (Multizone Adaptive Scheme for Transport and Phase Change Process). The scheme employs the curvilinear finite-volume approach for the discretization of the governing equations.
In a cylindrical coordinate system, conservation Eqs. (3) and (6) can be written in the general form as follows,

$$\frac{\partial}{\partial t}(rc\phi) = \frac{\partial}{\partial x}\left(r\Gamma \frac{\partial \phi}{\partial x} \right) + \frac{\partial}{\partial r}\left(r\Gamma \frac{\partial \phi}{\partial r} \right) + r(S_c + S_p \phi) \tag{13}$$

where ϕ is the generalized variable, Γ is the diffusion coefficient, and S_c is the volumetric source. The coefficient are defined as, c=0, $\Gamma = 1/\mu_m$, $S_c = J_0$, and $S_p = \varepsilon_m \omega^2 - i\omega\sigma_c - 1/r^2 (1/\mu_m)$ for magnetic vector potential equation ($\phi = A_0$); $c = (\rho c_p)_{eff}$, $\Gamma = k_{eff}$, $S_c = q_{eddy}^{'''} - (q_{radi}^{''} + q_{insu}^{''})\delta A / \delta V$, and $S_p = 0$ for energy equation($\phi = T$).
The grid used for the calculation is a structured trapezoidal mesh. For a typical primary point P, the conservation equation in a generalized coordinate system (ξ, η) can be written as,

$$\frac{\left(rc\phi Ja - r^0 c^0 \phi^0 Ja^0 \right)_P \Delta\xi\Delta\eta}{\Delta t} + r\left\{ \left(\alpha_\xi J_\xi \right)_e - \left(\alpha_\xi J_\xi \right)_w \right\} \Delta\eta +$$

$$r\left\{ \left(\alpha_\eta J_\eta \right)_n - \left(\alpha_\eta J_\eta \right)_s \right\} \Delta\xi = \left\{ r\left(S_c + S_p \phi \right) Ja + rS_\phi \right\} \Delta\xi\Delta\phi \tag{14}$$

where the curvature source term, S_ϕ, arises from the nonorthogonality of the grid,
$S_\phi = \left\{ \left(\beta_\xi J_\eta \right)_e - \left(\beta_\xi J_\eta \right)_w \right\} \Delta\eta + \left\{ \left(\beta_\eta J_\xi \right)_n - \left(\beta_\eta J_\xi \right)_s \right\} \Delta\xi$. α_ξ and β_ξ are the primary and the second area over the control volume face, e, respectively. J_ξ and J_η are the primary and the second flux over the control volume, e, respectively. For detailed definitions of these symbols, one can refer to [10].

The discretization equation for ϕ in the control volume surrounding point P can be written as,

$$a_P\phi_P = a_E\phi_E + a_W\phi_W + a_N\phi_N + a_S\phi_S + b \tag{15}$$

where $a_P = a_E + a_W + a_N + a_S + (rcJa/\Delta t - rS_P Ja)\Delta\xi\Delta\eta$,
$b = (r^0 c^0 Ja^0 / \Delta t\phi_P^0 + rS_c Ja + rS_\phi)\Delta\xi\Delta\eta$.

Magnetic field and temperature field can be obtained by solving the above equation.
In addition, the convergence of the numerical scheme is investigated here. Table 1 shows the dependence of temperatures on the iteration parameters, n_{time}. $T_{\max}$, T_{seed}, T_{charge} are the maxim temperature in the growth system, temperature of the SiC seed and temperature of the SiC charge, respectively; T_{top} and T_{bot} are the temperatures at the top hole and the bottom hole, respectively (see Fig. 1). As can be seen from Table 1, when the time step, *dt*, is less than 1, the temperatures converge to the same values. The iteration parameters, n_{time} have less effects on the calculation results when they are larger than 5.

Table 1. Dependence of temperatures on iteration parameters.

	$T_{\max}$	T_{seed}	T_{charge}	T_{top}	T_{bot}
dt=0.5, n_{time}=5	1784.6	1669.5	1713.4	1477.9	1688.9
dt=1, n_{time}=10	1784.5	1669.4	1713.3	1477.9	1688.9
dt=1, n_{time}=5	1784.5	1669.4	1713.3	1481.1	1692.9
dt=1, n_{time}=10	1784.5	1669.4	1713.3	1474.6	1684.8
dt=2, n_{time}=5	1784.2	1669.1	1713.0	1467.8	1676.4
dt=3, n_{time}=5	1657.6	1421.5	1488.4	881.4	1437.5
dt=5, n_{time}=10	1500.4	689.0	920.9	881.4	1437.5
dt=5, n_{time}=5	1500.1	688.8	920.6	881.3	1437.2

RESULTS AND DISCUSSIONS

The temperature distribution for current of 1500 A and frequency of 8 kHz is obtained. As can be seen in Fig. 2, the maximum temperature exists in the graphite susceptor at the level of the geometric center of the induction coil. The temperatures in the charge are higher than that near the seed, which allows the sublimation of SiC in the charge and deposition on the seed. At the seed surface, a positive radial temperature gradient is formed, which can initiate an outward growth and ensure the enlargement of the single crystal size [1].

1. Effects of Current on Temperature Distribution and Growth Rate Table 2 shows the temperatures and growth rates for different currents at frequency, f = 8 kHz. It can be seen that the temperatures and growth rates strongly depend on the current in the induction coil, which measures the power input to the growth system. The maximum temperature increases with the current. The temperature difference between the charge and the seed, however, remains unchanged. It can also be seen from Table 2 that the growth rate increases significantly with the current. For I = 1200 and 1300 A, the growth rates are very small, which may be attributed to the low temperatures in the growth systems. For I=1400 and 1500 A, the growth rates are much larger for pressure larger than 50 Torr. As can be seen, the growth rate decreases rapidly when the inert gas pressure increases.

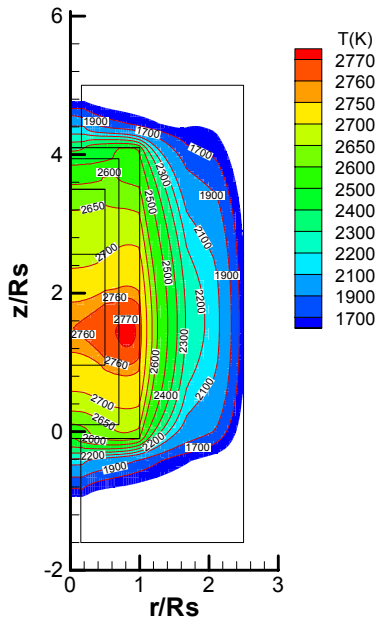

Fig.2 Temperature distribution for I=1500 A *and f=8* KHz

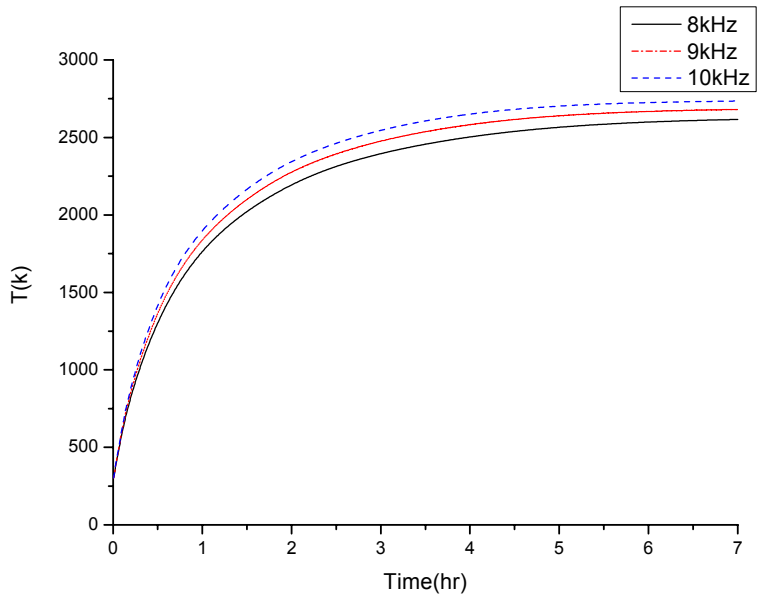

Fig.3 Evolution of the maximum temperatures with time for different frequencies

Table 2. Temperatures and growth rates for different currents, f = 8 kHz.

	T_{max}	T_{charge}	T_{seed}	T_{bot}	T_{top}	G (mm/hr, 50 Torr)	G (mm/hr, 75 Torr)	G (mm/hr, 100 Torr)
I=1200 A	2418	2324	2270	2234	1863	0.0112	0.0075	0.0056
I=1300 A	2552	2456	2406	2337	1969	0.0602	0.0399	0.0299
I=1400 A	2668	2567	2516	2422	2017	0.1979	0.1292	0.0960
I=1500 A	2775	2667	2616	2506	2054	0.6315	0.3943	0.2869

2. Effects of Frequency on Temperature Distribution and Growth Rate

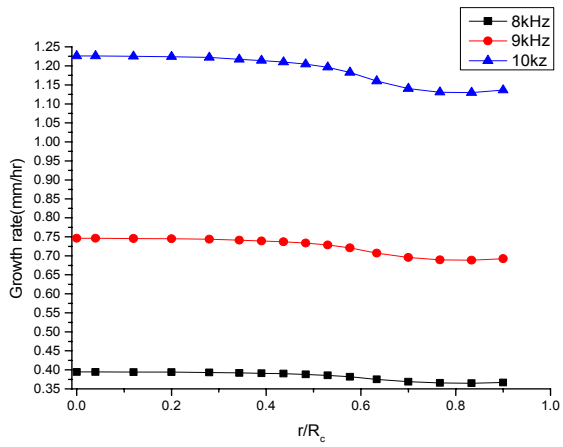

Fig.4 Predicted growth rates along the seed surface for different frequencies

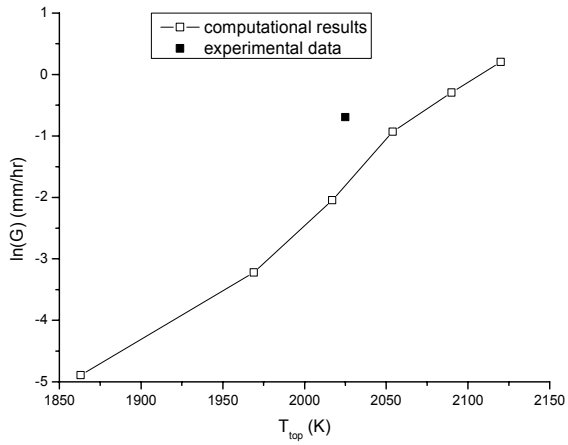

Fig. 5 The natural logarithm of growth rate versus top hole temperature

The evolution of maximum temperatures, T_{max} , for different frequencies during the heating stage is shown in Fig. 3. The temperatures stabilize after about 5 hours of heating. It can be seen that the maximum temperature increases with the frequency. It should be noted that the current in the coil, which is related to the voltage imposed on the coil, is limited. The temperature differences between different frequencies increase with time. When reaching the steady state, the maximum temperature for 9 kHz is about 65 K higher than that for 8 kHz, and 55 K lower than that for 10 kHz. Fig. 4 shows the predicted growth rates along the seed surface for different frequencies for the case of I=1500 A and inert gas pressure of 75 Torr. As can be seen, the growth rate increases rapidly with frequency. The growth rate decreases along the radial direction on the seed surface, which indicates that the crystal surface should be convex. This prediction is well proved by our experimental observations. Fig. 5 shows the dependence of growth rate on the top hole temperature. As can be seen, the natural logarithm is nearly proportional to the top hole temperature. The experimental data from our growth experiment coincides with the prediction, and the deviation shown in Fig. 5 may result from the error of the temperature measurement by pyrometer which bears an error margin of 5%.

CONCLUSION

A comprehensive process model has been developed to simulate the sublimation growth process of silicon carbide. The model accounts for the RF induction heating, heat transfer by conduction and radiation, mass transport and growth kinetics. The temperature distribution and growth rate are predicted for a 2-inch growth system. The dependence of temperature distribution and growth rate on the RF coil current is studied. It is found that the maximum temperature and growth rate increase rapidly with current. For $I < 1400A$, the growth rate is very small for pressure larger than 50 Torr. The dependence of temperature distribution and growth rate on induction frequency is also investigated in the paper. The temperature distribution and growth rate increase with frequency. The growth rate decreases along the radial direction, which indicates that the crystal surface should be convex. The dependence of growth rate on the top hole temperature is investigated, and the experimental data coincide with the prediction.

Acknowledges The research was supported by the Knowledge Innovation Program of Chinese Academy of Sciences, and the authors would like to thank Prof. V. Prasad at the Florida International University for helpful discussions.

REFERENCES

[1] Q.S. Chen, V. Prasad, H. Zhang,, M. Dudley, *Silicon carbide crystals — part II: process physics and modeling*, Crystal Growth Technology, K. Byrappa, T. Ohachi (Eds.), William Andrew/Springer-verlag, (2003).

[2] D. Hofmann, M. Bickermann, R. Eckstein, M. Kölbl, St.G. Müller, E. Schmitt, A. Weber, A. Winnacker, *Sublimation growth of silicon carbide bulk crystals: experimental and theoretical studies on defect formation and growth rate augmentation*, J. Crystal Growth, 198/199, (1999), 1005-1010.

[3] M. Pons, M. Anikin, K. Chourou, J.M. Dedulle, R. Madar, E. Blanquet, A. Pisch, C. Bernard, P. Grosse, C. Faure, G. Basset, Y. Grange, *State of the art in the modelling of SiC sublimation growth,* Materials Science and Engineering, B61-62, (1999), 18-28.

[4] St. G. Müller, R.C. Glass, H.M. Hobgood, V.F. Tsvetkov, M. Brady, D. Henshall, J.R. Jenny, D. Malta, C.H. Carter Jr., *The status of silicon carbide growth from an industrial point of view*, J. Crystal Growth, 211, (2000), 325-332.

[5] S.Yu. Karpov, A.V. Kulik, I.A. Zhmakin, Yu.N. Makarov, E.N. Mokhov, M.G. Ramm, M.S. Ramm, A.D. Roenkov, Yu.A. Vodakov, *Analysis of sublimation growth of bulk SiC crystals in tantalum container,* J. Crystal Growth, 211, (2000), 347.

[6] Q.S. Chen, H. Zhang, V. Prasad, *Kinetics and modeling of sublimation growth of silicon carbide bulk crystal***,** J. Crystal Growth, 224, (2001), 101-110.

[7] M. Selder, L. Kadinski, Yu. Makarov, F. Durst, P. Wellmann, T. Straubinger, D. Hofmann, S. Karpov , M. Ramm, *Global numerical simulation of heat and mass transfer fro SiC bulk crystal growth by PVT*, J. Crystal Growth, 211, (2000), 333-338.

[8] P. Råback, R. Nieminen, R. Yakimova, M. Tuominen, E. Janzén, *A coupled finite element model for the sublimation growth of SiC*, Materials Science Forum, 264-268, (1998), 65-68.

[9] R.H. Ma, H. Zhang, S. Ha, M. Skowronski, J. Crystal Growth 252, (2003), 523.

[10] Oszkár BíRó, Kurt Preis, *On the use of the magnetic vector potential in the finite element analysis of three-dimensional eddy currents*, IEEE Transactions on magnetics, 25, (1989), 3145-3159.

[11] Q.S. Chen, H. Zhang, V. Prasad, C. M. Balkas, N. K. Yushin, *Modeling of heat transfer and kinetics of physical vapor transport growth of silicon carbide crystals*, J. Heat Transfer, 123, (2001), 1098-1109.

[12] S.K. Lilov, *Study of the equilibrium process in the gas phase during silicon carbide sublimation,* Materials Science and Engineering, B21, (1993), 65-69.